



SIMULATION OF THE MAGNETOSPHERE WITH A NEW THREE DIMENSIONAL MHD CODE AND ADAPTIVE MESH REFINEMENT: PRELIMINARY RESULTS

D. S. Spicer,* S. T. Zalesak,* R. Löhner** and S. Curtis***

* NASA Center for Computational Sciences, NASA Goddard Space Flight Center, Greenbelt, MD 20771, U.S.A.

** Institute for Computational Sciences and Informatics, George Mason University, Fairfax, VA 22030, U.S.A.

*** Laboratory for Extraterrestrial Physics, NASA Goddard Space Flight Center, Greenbelt, MD 20771, U.S.A.

Abstract.

We present the first results from a new unstructured mesh three dimensional finite element MHD code which uses dynamic solution-adaptive mesh refinement in a manner similar to our two dimensional finite element MHD code /31/. The problem being considered here is the interaction of the solar wind with the earth's magnetosphere, using a three-dimensional Cartesian approximation. Our results strongly indicate that such adaptive mesh techniques have the ability to resolve structures in the three dimensional MHD flow field that would otherwise be possible only with orders of magnitude greater cost and that are most likely beyond the capability of present supercomputers.

1. Introduction

The existence of ubiquitous “boundary layers” in laboratory, Earth, space, and astrophysical phenomena makes the accurate modeling of these boundary layers nearly impossible in the context of a global solution using standard algorithms without enormous computational expense. Previously modellers had to be content to model a particular boundary layer separate from the global environment in order to provide a spatial grid adequate to resolve the phenomena. An example of this approach in space physics is the localized modelling of the magnetotail /1,2,3,4,5,6,7,8,9,10,11/. All of these efforts have improved our understanding of the phenomenon on a local scale. However, as the models used boundary conditions that did not accurately reflect the global evolution of the environment surrounding the boundary layer and could not account for the feedback from the boundary layer during its evolution, the resulting physical picture of how the boundary layer actually affected the global evolution was not entirely satisfactory as they were not self-consistent. Of course global magnetohydrodynamic (MHD) models of the magnetosphere have been in existence for well over a decade and have dramatically contributed to our understanding of how the solar wind couples with the earth's magnetic field to produce the magnetosphere and all its particulars /12,13,14,15,16,17,18,19,20,21,22,23,24,25/. Heretofore, the spatial resolution of these global models was limited by a combination of processor speed, memory size, and the availability of systems. While these limitations will always be with us, scientists being scientists, other approaches can help ameliorate the situation. One of these approaches is adaptive mesh refinement (AMR). AMR permits a fine numerical mesh where needed and nowhere else. In addition, the resolution of the mesh can be as high as one desires consistent with the physical approximation represented by the equations being solved. Finally, any parameter or combination of parameters can be used to determine the regions where refinement or de-refinement is desired. For these reasons AMR is ideal for modelling the complex flows that result when the solar wind forces the coupling of the interplanetary magnetic field, IMF, with the Earth's magnetic field and the resultant boundary layers.

Just as our approach differs from previous approaches to the global modelling of the magnetosphere in that we utilize AMR, our numerical scheme does likewise. Without exception all previous approaches have used finite volume or finite difference approximations

(12,13,14,15,16,17,18,19,20,21,22,23,24,25) while we utilize a finite element approach together with dynamic adaptive refinement of an unstructured mesh.¹ The combination of finite element and AMR on an unstructured mesh provides an extremely powerful tool for modeling the complex dynamics associated with the Earth's magnetosphere as well as irregularly shaped boundaries common to systems such as the Jupiter-Io system. In addition, the ability of the code to automatically make the mesh finer or coarser in response to the formation and movement of fine features in the flow field is an extremely powerful tool allowing us to compute a variety of physical phenomena very accurately, such as the current systems that result from the solar wind - magnetosphere interaction. In particular, the "boundary layers" such as the bow shock, the magnetopause, the magnetotail, and the polar cusp regions that characterize and to some degree control the global dynamics of the magnetosphere can be resolved in a manner heretofore not possible in global models of the magnetosphere, thereby permitting greater insight into the dynamics of the solar wind-magnetospheric coupling.

Further, the ability to resolve the flow field to any desired mesh size permits us to evaluate the applicability of the MHD approximation and the effect on the flow fields of adding terms to the MHD equations, such as the Hall term. In addition, because it is possible to resolve the gradients in the flow that characterize some of the instabilities believed to play a role in the dynamics of the magnetosphere, such as the Kelvin-Helmholtz/45/, lower hybrid drift (LHD)/41,42,43/, or the current convective instabilities in the magnetopause/44/, it is possible to compute the relevant stability parameters at each node, using the stability threshold conditions for the instability formulated in terms of fluid parameters. If the instability threshold conditions are found to be satisfied we can then change the appropriate transport coefficient, which are also parameterized in terms of fluid quantities, to account for the instability thereby allowing a test of the instability, and to compute observable characteristics.

The remainder of this paper is divided into three parts: a discussion of the model equations used and their limitations; a short summary of the finite element methodology; preliminary numerical results; and a discussion of our future plans for the code.

2. The Model Equations

As in any multi-dimensional MHD code the most difficult problem one must address first is how to transport the magnetic field, \vec{B} , in such a way that the constraint $\vec{\nabla} \cdot \vec{B} = 0$ is insured, or if not, that it be kept as small as possible so as not to generate significant magnetic monopoles and thereby measurably affect the solution. This requirement lead to the development of two versions of our 3D finite element MHD code, which we call FEMHD3D. One version we call the \vec{A} -code because we transport the vector potential \vec{A} using

$$\frac{\partial \vec{A}}{\partial t} = -\vec{E}, \quad (1)$$

where \vec{E} is the electric field, and then take its curl to obtain \vec{B} .² The other code we call the \vec{B} -code, because we transport \vec{B} directly in the conservative form

$$\frac{\partial \vec{B}}{\partial t} + \vec{\nabla} \cdot \vec{S} = 0, \quad (2)$$

where

$$S_{ik} = B_i v_k - B_k v_i - \frac{\eta c^2}{4\pi} \frac{\partial B_i}{\partial x_k}$$

¹ A structured mesh is one in which the neighbors of a grid point or cell are addressed by merely incrementing or decrementing the indices of an array. An unstructured mesh is one in which one is forced to maintain direct or indirect lists of neighbors for each cell or grid point. Also to avoid any confusion we want to emphasize that in his paper [24] Tanaka describes his mesh as being unstructured even though he is using a finite volume technique and the mesh is structured but non-uniform.

² Codes that use a staggered-mesh description of \vec{B} /15,26/ are effectively using a staggered vector potential evaluated at the same locations as \vec{E} .

and is derived using

$$\frac{\partial \vec{B}}{\partial t} = -c \vec{\nabla} \times \vec{E} \quad (3)$$

and Ohm's law

$$\vec{E} = -\frac{\vec{v} \times \vec{B}}{c} + \eta \vec{j}. \quad (4)$$

Each approach has its strengths and weaknesses. The obvious and most important reason for using the vector potential is that it guarantees $\vec{\nabla} \cdot \vec{B} = 0$ to round-off and that a very general Ohm's law can easily be implemented. The weakness with this approach is that while guaranteeing $\vec{\nabla} \cdot \vec{B} = 0$ everywhere within a tetrahedra, the current is discontinuous at the tetrahedra faces. This results in a noisy \vec{j} and difficulties in computing the divergence of the Maxwell stress tensor.

Transporting \vec{B} directly has none of the disadvantages associated with transporting \vec{A} and is easier to implement than transporting \vec{A} , but it does not guarantee \vec{B} satisfy $\vec{\nabla} \cdot \vec{B} = 0$, which is a non-trivial concern. Because $\vec{\nabla} \cdot \vec{B} = 0$ is not guaranteed when \vec{B} is transported directly, the MHD equations cannot be cast into conservative form. To take account of this problem various authors /27,28,29/ have used simple mathematically motivated tricks that correct \vec{B} so that $\vec{\nabla} \cdot \vec{B} \simeq 0$ to some order of accuracy. In the \vec{B} -code we have adapted the approach of Schmidt-Voigt /28,29/, which is to add $-\vec{v} \vec{\nabla} \cdot \vec{B}$ as a source term to (2). This has the effect of transporting any magnetic monopoles out of the region in which they develop. Unfortunately in regions where the field lines are closed this trick is not as effective. Schmidt-Voigt /29/ uses a metric for determining how good \vec{B} satisfies $\vec{\nabla} \cdot \vec{B} = 0$, which is $\omega = |\delta x| |\vec{\nabla} \cdot \vec{B}| / |\vec{B}|$. Schmidt-Voigt insists ω be less than 10^{-5} even though his results show no obvious effects due to monopoles until $\omega \approx 10^{-2}$. We find $\omega \approx 10^{-5}$ even without AMR. With AMR \vec{B} satisfies $\vec{\nabla} \cdot \vec{B} = 0$ even better in those regions where refinement occurs as expected from Schmidt-Voigt's error criterion. Thus, AMR helps alleviate the problem with the divergence of \vec{B} and our results to date show no obvious effects due to the existence of magnetic monopoles. Another trick used is to correct the magnetic field by the technique of projection, first discussed by Brackbill and Barnes /27/, and used by Schmidt-Voigt /29/ and Tanaka /25/. To date we have not implemented this technique. In a separate paper we plan to directly compare \vec{B} obtained from the \vec{A} -code and \vec{B} -code.

The other equations being solved are the familiar continuity, momentum, and energy equations:

$$\frac{\partial \rho}{\partial t} + \vec{\nabla} \cdot (\rho \vec{v}) = 0 \quad (5)$$

$$\frac{\partial(\rho \vec{v})}{\partial t} + \vec{\nabla} \cdot (\rho \vec{v} \vec{v}) = -\vec{\nabla} P + \frac{\vec{j} \times \vec{B}}{c} \quad (6)$$

$$\frac{\partial \mathcal{E}}{\partial t} + \vec{\nabla} \cdot (\mathcal{E} \vec{v}) = -\vec{\nabla} \cdot (P \vec{v}) + \vec{j} \cdot \vec{E} \quad (7)$$

with the gas dynamic energy \mathcal{E} given by

$$\mathcal{E} = \frac{1}{2} \rho \vec{v}^2 + \frac{P}{\gamma - 1} \quad (8)$$

These equations are supplemented with Ampere's equation

$$\vec{\nabla} \times \vec{B} = \frac{4\pi}{c} \vec{j} \quad (9)$$

from which follows the conservative form of the Lorentz force

$$\frac{\vec{j} \times \vec{B}}{c} = \frac{1}{8\pi} \vec{\nabla} \cdot (2\vec{B}\vec{B} - B^2). \quad (10)$$

In the above, ρ , \vec{v} , P , \mathcal{E} , and \vec{J} are respectively the mass density, the bulk flow velocity, the scalar plasma pressure, the total plasma gasdynamic energy, and the current density. Note that we are using the gasdynamic energy rather than the total energy, and that Ohm's law can be considerably more complex for the \vec{A} -code version of FEMHD3D in these specific calculations. The use of the gasdynamic plasma energy rather than the total energy

$$\mathcal{E}_T = \frac{1}{2}\rho\vec{v}^2 + \frac{P}{\gamma - 1} + \frac{B^2}{8\pi} \quad (11)$$

is dictated by the fact that the magnetic energy near the Earth is many orders of magnitude larger than either the internal energy or the ram pressure there. As a result truncation errors occur when these two large numbers are subtracted from one another to obtain

$$P = (\gamma - 1)\left(\mathcal{E}_T - \frac{1}{2}\rho\vec{v}^2 - \frac{B^2}{8\pi}\right)$$

leading to negative pressures.

3. Finite Element Methodology

FEMHD3D is a modular enhancement of the FEFLO family of codes [33,34,35,36]. These codes solve the equations of compressible gasdynamics (*i.e.*, the MHD equations above in the limit of $\vec{B} = 0$) with *no symmetries* imposed on the solutions. The basic technique employed is the two-step Taylor Galerkin method on a mesh consisting of tetrahedra in 3D. Although these codes have many capabilities, our interest here is on two of them: 1) dynamic, solution-adaptive mesh refinement capabilities; and 2) shock-capturing capabilities.

First and foremost, we feel strongly that dynamic, solution-adaptive mesh refinement, which we have been simply calling "AMR", is absolutely necessary if we are to be able to resolve the disparate scale sizes that arise in many problems, including the magnetospheric problem being addressed here. To simultaneously resolve the smallest scale sizes of interest (*e.g.*, the details of the magnetotail), and also represent the global morphology of the entire magnetosphere, is presently out of the question even for the most imaginative of static mapped meshes. Our approach to solving this difficulty is AMR. The AMR philosophy is implemented by starting with a very coarse mesh, and then recursively dividing cells (tetrahedra in this case) into smaller and smaller cells until acceptable local levels of accuracy are achieved. Of course, one must also have the ability to "un-refine" the mesh when there is no longer a need for the existing level of refinement. The basic ideas behind AMR are not new (see [37] for example), but the last decade has seen much use of the idea both for structured grids (*e.g.*, [38]) and unstructured grids (*e.g.*, [34]).

The second capability of interest is shock-capturing. While AMR addresses the ability to resolve small scale structures of interest it is of no interest to refine to scales below the physical validity of the equations being solved, here the ideal MHD approximation. We use the term "shock" to denote any sharp feature of the flow that is so small that the approximation we are using is no longer valid. The Earth's bow shock is a simple example, since it is in reality a collisionless shock for which MHD provides only upstream and downstream information across the shock but nothing about its structure. The basic idea of shock-capturing methods is to locally add just enough numerical dissipation in the vicinity of the "shock" to smear it over a small number of cells. (Note that in some sense this is the inverse of AMR: we are adjusting the solution to the mesh rather than the mesh to the solution.) The technique employed in the FEFLO family, and hence in FEMHD3D, is the multidimensional flux-corrected transport (FCT) algorithm developed by Zalesak [39], and modified by Löhner *et al.* [33] for gasdynamics on an unstructured finite element mesh.

The process of converting FEFLO to FEMHD3D was essentially straight forward and consisted of four steps: 1) adding a time evolution equation for the magnetic field (Eq.(1) or (2)), which we have already discussed; 2) adding the Lorentz force term to Eq.(6); 3) adding the $\vec{J} \cdot \vec{E}$ term to Eq. (7); and 4) formulating a set of criteria for the refinement and de-refinement process.

In advancing the momentum equation Eq.(6), the conservative form of the Lorentz force Eq. (10) is preferable, since it can guarantee that momentum be conserved numerically. However, this

form leads to truncation errors which can give rise to finite components of the force along the magnetic field. We remove all components of the Lorentz force parallel to \vec{B} at each time step, recognizing the loss of exact momentum conservation in the affected regions.

The addition of the $\vec{J} \cdot \vec{E}$ term to Eq. (7) was done so as to guarantee the internal energy is not changed except through Ohmic heating.

Finally, we need a way of deciding when and where to refine and de-refine the mesh for the earth's magnetosphere. As noted in the introduction we can refine and de-refine based on any parameter or set of parameters we like. However, as we want to resolve simultaneously as many of the boundary layers as possible that characterize the magnetosphere, physics dictates that we chose parameters that characterize these boundary layers observationally. As the bow shock, magnetosheath, magnetopause and magnetotail all produce characteristic magnetic field rotations across these layers it is the current density and its sources that we are naturally lead to as refinement parameters. In 2D /38,39/ and 3D one refinement parameter that was found to be effective is

$$R = |\vec{\nabla} \times \vec{B}| / |\vec{B}|, \quad (12)$$

which relates rapid spatial variations in \vec{B} relative to its magnitude. The mesh that results from utilizing (12) is shown in Figure (1).

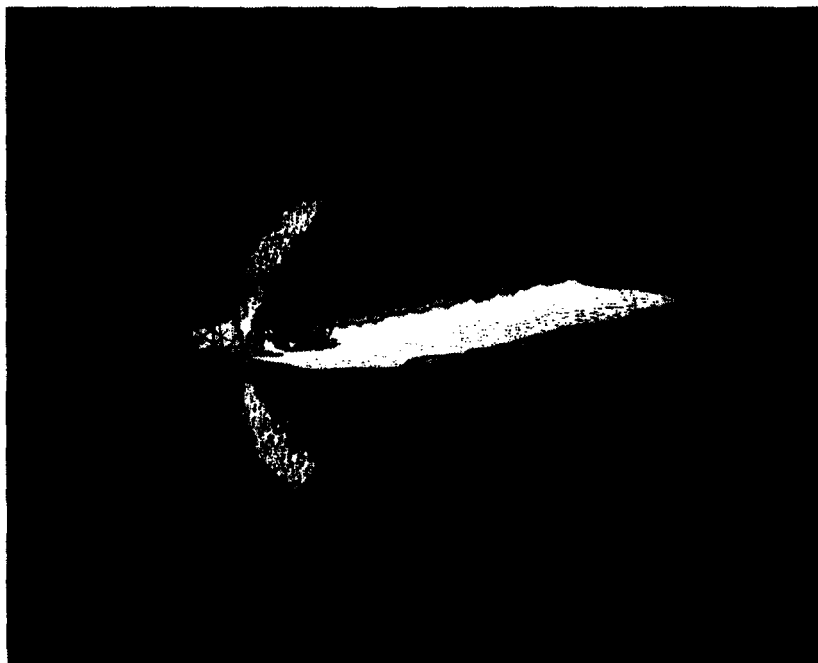


Fig. 1 Regions where mesh has been refined using $R = |\vec{\nabla} \times \vec{B}| / |\vec{B}|$ as the refinement parameter. The complicated irregular spacing of the triangles in the x - y and x - z planes is due to the orthogonal slices through the refined tetrahedral mesh.

Before refinement the mesh had a maximum spatial scale length of $12R_E$ and a minimum spatial scale length of $0.75R_E$. The entire mesh consisted of 14,000 points or if the mesh were the same extent in all directions roughly 24^3 points, which would be a very coarse mesh if the mesh were uniform. After refinement the maximum spatial scale length remains the same but the minimum spatial scale length becomes $0.1R_E$ so that the entire mesh consisted of 33,000 points or if the mesh were the same extent in all directions roughly 32^3 points. If we ignore the Earth

the shape of the refined region using R is shaped like a mushroom with the head of the mushroom on the day with an envelope that includes the bow shock and magnetopause. The stalk of the mushroom has the shape of two lobes, one on the dusk side and the other on the dawn side, with a thinner region bridging the two. As one moves further back into the tail the lobes get broader and the bridge thicker.

To have a uniform spatial resolution of $0.1R_E$ within a box $150 \times 120 \times 120 R_E^3$ would require a mesh made up of 10^9 points which is impossible with today's computers. Even a non-uniform static mesh with regions of high resolution, which were chosen judiciously, would still be of the order 10^6 points but still not have the resolution achievable with AMR, since AMR will cause the mesh to change as the flow evolves. In the case of the magnetosphere it might be argued that the coupled system is near steady state so that one could use a static mesh. This argument is valid as long as one is not interested in following the dynamics of the flow that results from reconnection which is clearly not a steady state phenomena. Further solar activity leads to transients that result in transient activity within the magnetosphere. Such activity and where it will occur within the magnetosphere cannot a priori be predicted so that even the most ingenious non-uniform static meshes will have difficulty treating all cases of a realistic dynamic magnetosphere.

Another parameter that appears to be useful for refinement is the vorticity, $\vec{\Omega} = \vec{\nabla} \times \vec{v}$. As is well known temporal variations in $\vec{\Omega}$ act as source terms for field aligned currents. As shown in Figure (2) the vorticity has a complex structure both in the meridional plane ($y=0$ plane) and equatorial planes ($z=0$ plane). In the meridional plane Ω_y and equatorial plane Ω_z has fine structure both above and below the plasma sheet. As is evident from Figure (2) the region in the tail corresponding to the flux-rope has fine structure indicating the a rotation of the flux-rope. There is also evidence of significant vorticity at the edge of the magnetopause which supports the suggestion that the Kelvin-Helmholtz instability might be operational there. As vorticity represents the local and instantaneous rate of rotation of the fluid one cannot conclude from the figure the time behaviour of \vec{v} but our results show that the vorticity pattern approaches a quasi-steady state except during reconnection. Hence, Ω appears to be a useful refinement parameter.

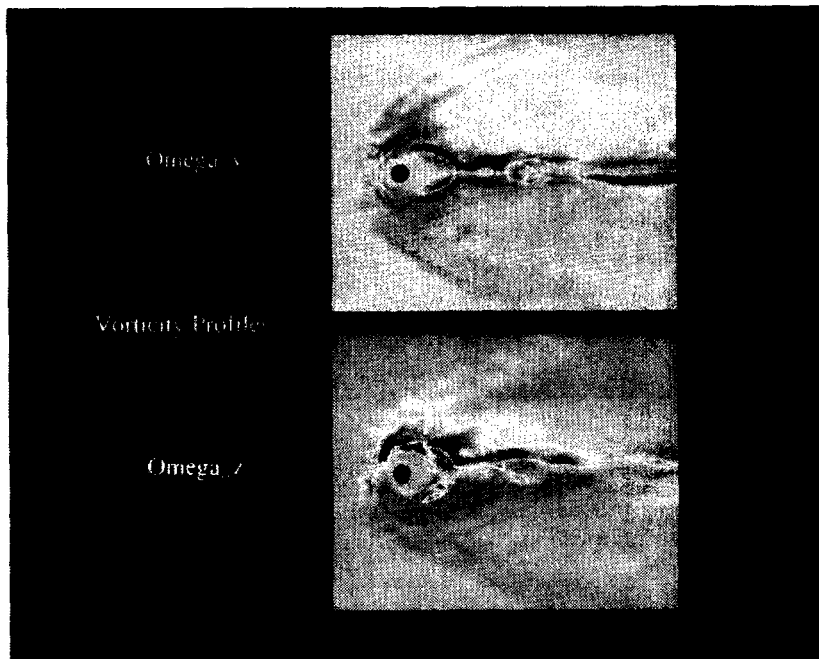


Fig. 2 Vorticity shown in the Meridional and equatorial planes. Changes in color indicate changes in direction.

4. Numerical Results

As noted above the calculation discussed in this section was performed in a box of $150 \times 120 \times 120 R_E^3$ on each side. The inner boundary was treated as a perfectly conducting sphere of radius $3.7 R_E$. A 3D dipole magnetic field normalized to have a magnitude of $0.5 G$ at a radius of $1 R_E$ was used as the initial condition. The solar wind was initialized globally with a speed of 400 km/s , a density of 5 cm^{-3} , and a temperature of $10^5 K$. This initial wind speed was gradually decreased to zero in the immediate vicinity of the earth. Initially the embedded solar wind field was set to zero over the domain, but this was quickly replaced by the $5 \times 10^{-5} G$ southward field set at the left boundary.

Probably the most significant result to date using FEMHD3D is the three dimensional topology of the magnetotail that results from reconnection. It is clearly obvious from either version of FEMHD3D that the structure resulting from reconnection is not 2D but 3D in nature and confirms numerically the predictions of Hughes and Sibeck /32/. While we can't yet fully confirm the dynamics predicted we can confirm the topology of the field lines is that of an open helix and not loops of closed field lines as the 2D model would predict. The helix extends roughly symmetrically in the dawn-dusk direction with the helix pitch smallest near the dawn-dusk symmetry plane and the pitch getting larger as one moves either in the dawn or dusk direction. In addition, each end of the helix connects to a hemisphere of the Earth. Open field lines are topologically wrapped in a helix about the helix that connects to the Earth. To be able to better understand the dynamics of these helices, or flux ropes as they are called by Hughes and Sibeck/32/, requires the making of a movie so that we can watch the evolution from different angles.



Fig. 3 Typical magnetic field structure obtained from FEMHD3D in the meridional plane. Notice the knot of field lines which appears as a 2D plasmoid as an artifact of the projection.

Figure (3) illustrates the magnetic field lines that result from a typical simulation. There is a tight knot of field lines in the magnetotail and these field lines do not all lie in the meridional plane, as is usually depicted. Figures (4), (5), and (6) provide a close up view of the knot. Figure (4) is a view of the knot in the dawn to dusk direction. As is evident the helix spirals tighter as

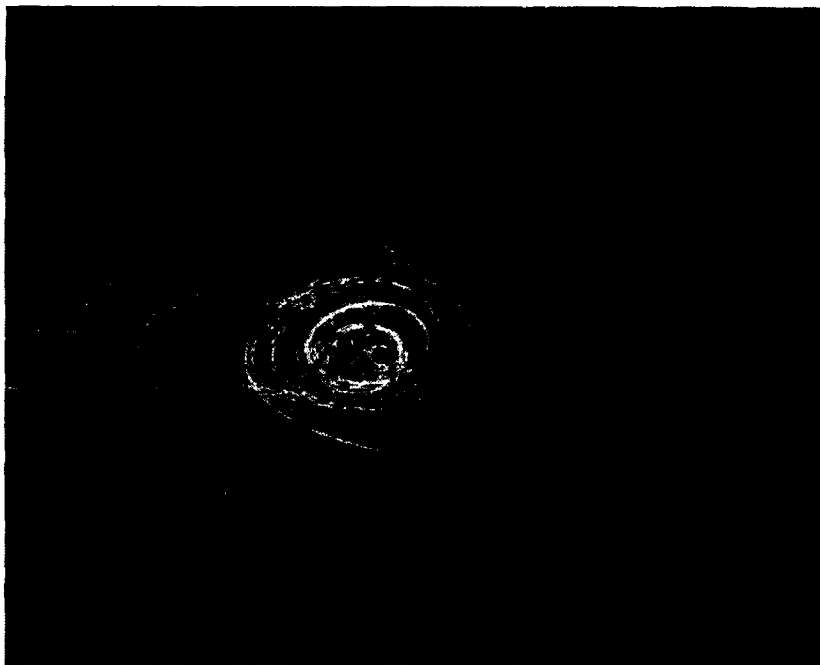


Fig. 4 *A blow up view of the knot of field lines as viewed in the dawn to dusk direction through the meridional plane. The is to the left.*

one moves from the outside in. Figure (5) is a view looking at the equatorial plane. The helical behaviour of the field lines becomes even more obvious, while Figure (6) is a view from $\approx 45^\circ$ above the equatorial plane. We should emphasize that the mesh used to generate these plots did not possess adequate resolution (33,000 points) throughout the domain of the knot so that the knot may be smaller in practice than our plots indicate.



Fig. 5 *A blow up view of the knot of field lines as viewed looking normal to the equatorial plane.*

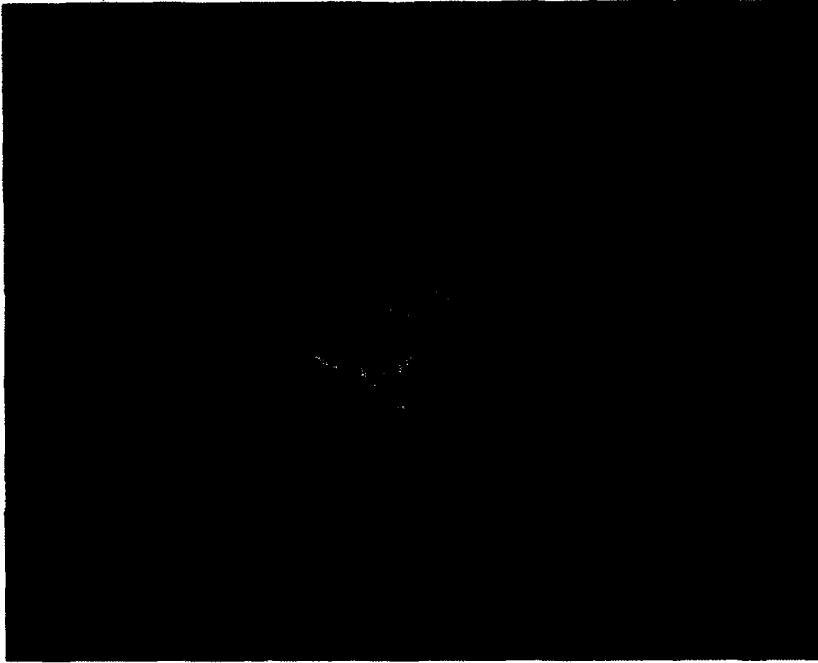


Fig. 6 A blow up view of the knot of field lines as viewed approximately 45° above the equatorial plane.

5. Discussion

It is our belief that the preliminary 3D results presented here amply illustrate the power of AMR. We need to complete a series of tests before we declare FEMHD3D fully operational and ready for production runs. In addition, we need to add an ionospheric model to the code to better represent the inner boundary conditions. This we are presently working on. A future study will include attempts to include a ring current system. Finally we need to investigate better techniques for displaying and interpreting the complex flows that result from 3D simulations.

Acknowledgements

Computations were performed on both the NASA/GSFC NCCS Cray C98 and the NASA/Ames NAS Cray C90 systems.

References

- [1] Hayashi, T. and T. Sato, 1978. *J. Geophys. Res.*, **83**, 217
- [2] Sato, T., T. Hayashi, T., T. Tamao, and A. Hasagawa, 1978. *Phys. Rev. Lett.*, **41**, 1548
- [3] Sato, T., T. Hayashi, 1979. *Phys. Fluids.*, **22**, 1189
- [4] Lebeouf, J.N., T. Tajima, C.F. Kennel, and J.M. Dawson, 1978. *J. Geophys. Res. Lett.*, **5**, 609
- [5] Ugai, M. and T. Tsada, 1977. *J. Plasma Phys.* **17**, 337
- [6] Tsada, T. and M. Ugai, 1977. *J. Plasma Phys.* **18**, 451
- [7] Birn, J., 1980. *J. Geophys. Res.*, **85**, 1214
- [8] Scholer, M., 1987. *J. Geophys. Res.*, **92**, 12425
- [9] Forbes, T. and E. R. Priest, 1983. *Solar Phys.*, **84**, 169
- [10] Birn, J. and K. Schindler, 1985. *J. Geophys. Res.*, **90**, 3441
- [11] Birn, J., E.W. Hones, and K. Schindler, 1986. *J. Geophys. Res.*, **91**, 11116

- [12]Brecht, S.H., J.G. Lyon, J.A. Fedder, and K. Hain, 1981. *J. Geophys. Res. Lett.*, **8**, 397
- [13]Brecht, S.H., J.G. Lyon, J.A. Fedder, and K. Hain, 1982. *J. Geophys. Res.*, **87**, 6098
- [14]LeBoeuf, J.H., T. Tajima, C.F. Kennel, and J.M. Dawson, 1981. *J. Geophys. Res. Lett.*, **8**, 257
- [15]Lyon, J., S.H. Brecht, J.A. Fedder, and P.J. Palmadesso, 1980. *J. Geophys. Res. Lett.*, **7**, 721
- [16]Lyon, J., S.H. Brecht, J.D. Huba, J.A. Fedder, and P.J. Palmadesso, 1981. *Phys. Rev. Lett.*, **46**, 1038
- [17]Schmidt, H.U. and R. Wegman, 1980. *Comp. Phys. Comm.*, **19**, 309
- [18]Wu, C.C., R.J. Walker, and J.M. Dawson, 1981. *J. Geophys. Res. Lett.*, **8**, 525
- [19]Watanabe, K. and T. Sato, 1990. *J. Geophys. Res.*, **95**, 75
- [20]Ogino, T., 1986. *J. Geophys. Res.*, **91**, 6791
- [21]Ogino, T., R.J. Walker, M. Ashour-Abdalla, J.M. Dawson, 1986. *J. Geophys. Res.*, **91**, 10029
- [22]Watanabe, K. and T. Sato, 1988. *J. Geophys. Res. Lett.*, **15**, 717
- [23]Usadi, A. and A. Kageyama, K. Watanake, and T. Sato, 1993. *J. Geophys. Res.*, **98**, 7503
- [24]Tanaka, T., 1992. *Comp. Fluid Dynamics. J.*, **1**, 14
- [25]Walker, R.J., T. Ogino, J. Raeder, and M. Ashour-Abdalla, 1993. *J. Geophys. Res.*, **98**, 17235
- [26]Evans, C.R. and J.F. Hawley, 1988. *Astrophys. J.*, **332**, 659
- [27]Brackbill, J.U. and D.C. Barnes, 1980. *J. Comp. Phys.*, **35**, 426.
- [28]Schmidt-Voigt, M., 1987, in *Intersellar Magnetic Fields*, eds. R. Beck, R. Gräve, P.251, Springer, Berlin Heidelberg New York .
- [29]Schmidt-Voigt, M., 1989. *Astr. Astrophys.*, **210**, 433
- [30]Brackbill, J., 1985. *Space Sci. Rev.*, **42**, 153
- [31]Zalesak, S.T., D.S. Spicer, R. Löhner, and S.Curtis, 1993, in *Spatio-Temporal Analysis for Resolving Plasma Turbulence (START)*, eds. A. Roux, F. Lefeuvre and D. LeQueau, P. 315, ESA WPP-047 .
- [32]Hughes, W.J. and D.G. Sibeck, 1987. *J. Geophys. Res. Lett.*, **14**, 636
- [33]Löhner, R., Morgan, K. and Zienkiewicz, O.C., 1984. *Int.J.Num.Meth.Fluids*, **4**, 1043.
- [34]Löhner, R., Morgan, K., Peraire, J. and Zienkiewicz, O.C., 1985. *AIAA*, **85**, 1531-CP.
- [35]Löhner, R., 1987. *Comp.Meth.Appl.Mech.Eng.*, **61**, 323.
- [36]Löhner, R., 1989. *AIAA*, **89**, 0365.
- [37]Phillips, N., and Shukla, J., 1973. *J. Appl. Met*, **12**, 763.
- [38]Berger, M., and Olinger, J.. *J. Comp. Phys.*, **53**, 484.
- [39]Zalesak, S.T., 1979. *J. Comp. Phys.*, **31**, 335.
- [41]Huba, J.D., N.T. Gladd and K. Papadopoulos, 1977. *J. Geophys. Res. Lett.*, **4**, 125
- [42]Gary, S.P. and T.E. Eastman, 1979. *J. Geophys. Res.*, **844**, 7378
- [43]Gary, S.P. and A.G. Sgro, 1990. *J. Geophys. Res. Lett.*, **17**, 909
- [44]Drake, J.F., J. Gerber, and R.G. Kleva, 1993. .
- [45]Haerendel, G. and G. Paschmann, 1982, in *Magnetospheric Plasma Physics*, ed. A. Nishida, D. Reidel Publishing Company .